EFFECT OF PLY THICKNESS AND CONSTITUENTS ON THE TRANSVERSE CRACK PROPAGATION OF THIN-PLY COMPOSITES: DAMAGE PROGRESSION AND MODELLING

S. Kohler[1], J. Cugnoni[1] and J. Botsis[1]

[1]LMAF, Faculté des sciences et techniques de l'ingénieur, Ecole Polytechnique Fédérale de Lausanne (EPFL), Bâtiment ME, Station 9. CH-1015 Lausanne, Switzerland
Email: sebastien.kohler@epfl.ch, Web Page: http://lmaf.epfl.ch

Keywords: Thin-ply, Tomography, Mechanical testing, Finite element analysis, Multiscale modelling

Abstract
Quasi-isotropic thin-ply CFRP specimen made out of two different fibre/matrix systems and selected ply thicknesses were tested to monitor the appearance and propagation of damage at the free edges and in the bulk. A multi-scale embedded cell FE model was developed for one of these systems to further understand the mechanisms at play and its results were compared with the experimental ones. The use of an acoustic emission cumulative energy threshold was validated by tomographic imaging, as well as the delaying of free edge damage propagation into the bulk of the samples with reducing ply thickness.

1. Introduction

Thin-ply composites have attracted a lot of attention since the emergence of modern tow-spreading techniques due to the improvement of several mechanical properties offered by this new class of materials, coupled with a much increased design space for some applications. Unfortunately, the prediction of the extent of this increase has proved difficult to realise in some instances, as significant discrepancies have been observed between experimental results and the LEFM based in-situ strength model [1] for very thin plies, as shown by Amacher et al. [2]. This study provides a step towards the understanding of the underlying mechanisms which control the increase of transverse strength properties of these novel materials. Specifically, two prepreg systems are investigated with respect to free edge and bulk damage, through the use of optical microscopy, acoustic emission and X-Ray tomography.

The different experimental damage indicators are compared, highlighting that free edge damage and bulk damage are two separate mechanisms following their own scaling with ply thickness. Free edge effects dominate the behaviour of samples made of thick ply materials, whereas their propagation into the bulk of the samples is delayed for samples made of thinner plies. The experimental results are also compared with a multiscale FE model using microstructures based on the actual samples tested. A parallel is then drawn between the numerical results and the analytical in-situ strength model. The results point towards the existence of an "in-situ G_{IC}" value which is a function of ply thickness.

2. Materials and Methods

In this study, two different prepreg systems produced by North Thin Ply Technology, Lausanne Switzerland, were investigated, namely a rather brittle, low TG TP80ep resin coupled with high modulus Toray M40JB fibres, and another designed for the aerospace industry with a high TG

toughened TP175ep resin and high strength Toray T800 fibres. Quasi-isotropic ($[45/90/-45/0]_{ns}$) tensile samples were produced accordingly to the ASTM D3039 standard out of several different ply thicknesses for each material. By varying the number of repetitions *n* of the sub-laminate, a similar sample thickness was targeted for all the different ply thicknesses used for a given material, allowing a study of the ply thickness effect only. The autoclave curing followed the manufacturer's recommended curing cycles for both resins and took place in an aluminium mould to ensure a good planeity of the samples. A fibre volume fraction of 55% was targeted for all cases. Tapered tabs made of 2mm thick ±45° GFRP were glued on the extremities of the samples and HBM LY41/6-120 strain gauges installed in the middle of the gauge length. Details regarding the samples, including the gsm designation relationship with ply thickness, can be found in Table 1. It has to be noted that the 300gsm plies for the M40/TP80 system were made by restacking two 150gsm plies. The same procedure was followed for the preparation of 134gsm and 268 gsm samples for the T800/TP175 system due to production constraints.

Table 1: Sample description

Samples	Fibres	Matrix	Ply t. (µm)	*n* (-)	Sample t. (mm)	V_f (%)
300gsm	M40JB	TP80ep	297.62	1	2.32 ± 0.030	59
150gsm	M40JB	TP80ep	148.81	2	2.32 ± 0.016	57
100gsm(*)	M40JB	TP80ep	99.87	4	3.21 ± 0.032	56
75gsm	M40JB	TP80ep	75.13	4	2.41 ± 0.035	56
30gsm	M40JB	TP80ep	30.06	10	2.52 ± 0.064	52
268gsm	T800	TP175ep	260.96	1	1.95 ± 0.022	60
134gsm	T800	TP175ep	130.48	2	1.88 ± 0.011	62
67gsm	T800	TP175ep	65.24	4	1.92 ± 0.015	61
34gsm	T800	TP175ep	32.58	8	2.19 ± 0.016	53

(*) Used only for tomography in this study

Before testing, the samples were polished on one of their free edges to allow in-situ optical microscopic observations to take place during the test. In the case of the M40/TP80 system, an Edmund Optics binocular microscope and Guppy-Pro camera were used to monitor damage at the free edges. For the T800/TP175 system, a Keyence VHX-5000 microscope was used instead. In both cases, the point at which the first damages occurred, their nature and development as well as free edge crack density were recorded. Due to the time taken by the image acquisition process, and in order to guarantee a good temporal resolution of the images, a slower loading rate than proposed by the testing standard was used, i.e., at 0.125mm/min.

Additionally, the acoustic emission produced during the testing of such samples was recorded using a *Mistras-2001* acoustic emission acquisition setup. A threshold, set empirically on the cumulative acoustic energy recorded, was defined as a damage predictor, as had been done previously on the same M40/TP80 material [2-3].

In order to study the damage propagation from the free edge into the bulk, some additional samples were tested using the same loading rate as during the previous experiments, but only until load levels deemed interesting, between the appearance of free edge cracks but before the acoustic emission was reached, or just after this threshold was reached. The tests were then promptly interrupted and the samples unloaded. Tomographic images of these partially loaded samples were then taken on a RX-Solutions Ultratom micro CT scanning device, where the resolution of approximately 7µm per voxel allowed the observation of 10mm of gauge length over half the width of the sample for each scan. The micro-damage detection at this resolution was made possible by the use of a ZnI_2-based penetrant solution which has been shown to produce good contrast [4] and has the additional benefit to free the

imaging process from time constraints as the iodide compounds formed in the solution stay in the sample even after evaporation of the solution. In order to ensure a good penetration of this contrasting agent, it was applied during 24 hours on slightly (typically 50MPa) reloaded samples to reopen the cracks previously created during the test.

An embedded cell, multiscale FE model (Fig. 1) was used to study the mechanisms observed experimentally. Pictures from the actual microstructures of the M40/TP80 system in three different ply thicknesses were used to model the embedded cell representing a portion of a 90° ply, which is surrounded by 4 linear elastic homogenized plies. The lamina properties of these homogenized plies can be found in [2]. The sides are forced to remain planar for plane strain conditions or are left free to approximate plane stress state. The fibres were modelled as isotropic elastic solids using manufacturer-provided properties, whilst the fibre-matrix interface relied upon a linear softening, energy-based cohesive model. The matrix is modelled with a hyperbolic Drucker-Prager model with regularized damage and associated flow rule. The yield properties were obtained by experimental uniaxial tensile and compressive testing of neat resin samples, yielding a β angle of 35°. The initial hydrostatic tensile strength of 35 MPa was determined by using the yield model proposed by Melro et al. [5] with the experimentally obtained yield values. A transition zone, shown in lighter red on Fig. 1, was defined at the sides of the embedded cell, where the material properties were gradually changed to smooth out the transition to the surrounding plies and thus avoid any localization. All the results were evaluated outside of this transition zone. The problem was solved using a dynamic explicit solver (Abaqus© Explicit) with convergence studies performed on both the mass scaling parameter and the mesh.

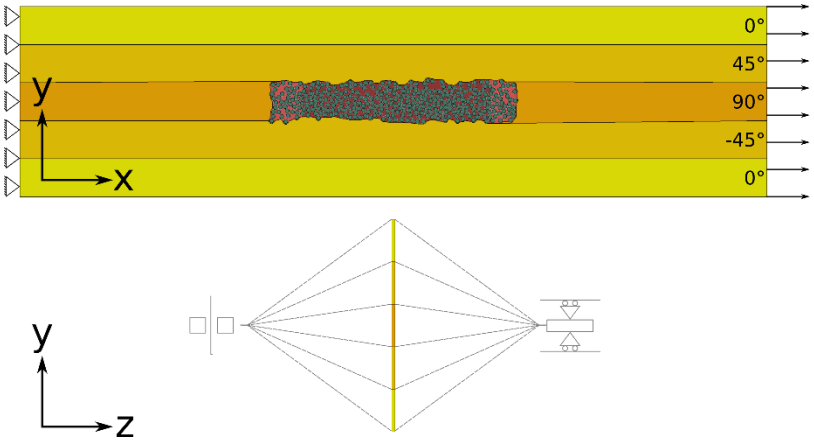

Figure 1: Description of the FE model

This model proved to be only weakly sensitive to the interface strength parameter used, which was set at 20 MPa by an inverse identification process of the experimental transverse tensile strength (ASTM D3039 90° unnotched tensile tests) value by using an RVE containing 180 randomly placed fibres for an equivalent fibre volume fraction as in the experimental test. On the other hand, the model was most sensitive to the interface toughness parameter, which was identified at 7.5 J/m^2 for the samples made with 150 micron plies by fitting the macroscopic stress at which the first crack observed numerically appeared with the stress at which the acoustic emission threshold was reached. These material properties were then kept constant for the simulations involving other ply thicknesses.

An in-situ G_{IC} value could be determined from the simulation results by summing the increment of plastic and damage dissipation energy in the embedded cell during the development of the first crack. By dividing the dissipated energy increment by the surface of crack formed, an in-situ energy release rate could be computed for the transverse cracking mechanism.

3. Results

The damage mechanisms are observed to change notably with decreasing ply thickness. In the case of the M40/TP80 system, the first transverse cracks appear around 0.32% strain for the 300gsm samples, together with occasional secondary delaminations and some intra-ply delamination at the re-stacking interface between the two 150gsm plies. Matrix-cracking induced delamination is then quickly triggered from 0.5% strain onwards until the sample fails due to large scale delamination around 0.8% strain. The 150gsm samples on the other hand only show the first transverse cracking around 0.45% strain with much more limited delamination than in the previous case appearing past 0.8% strain until the specimen failure. The 75gsm samples are observed to have a higher onset of transverse cracking than specimen made out of thicker plies, with no apparent damage until 0.54% strain on average. However, no delamination could be seen in this case until specimen failure. Finally, no damage could be observed for the 30gsm samples with the resolution of the set-up used for these samples.

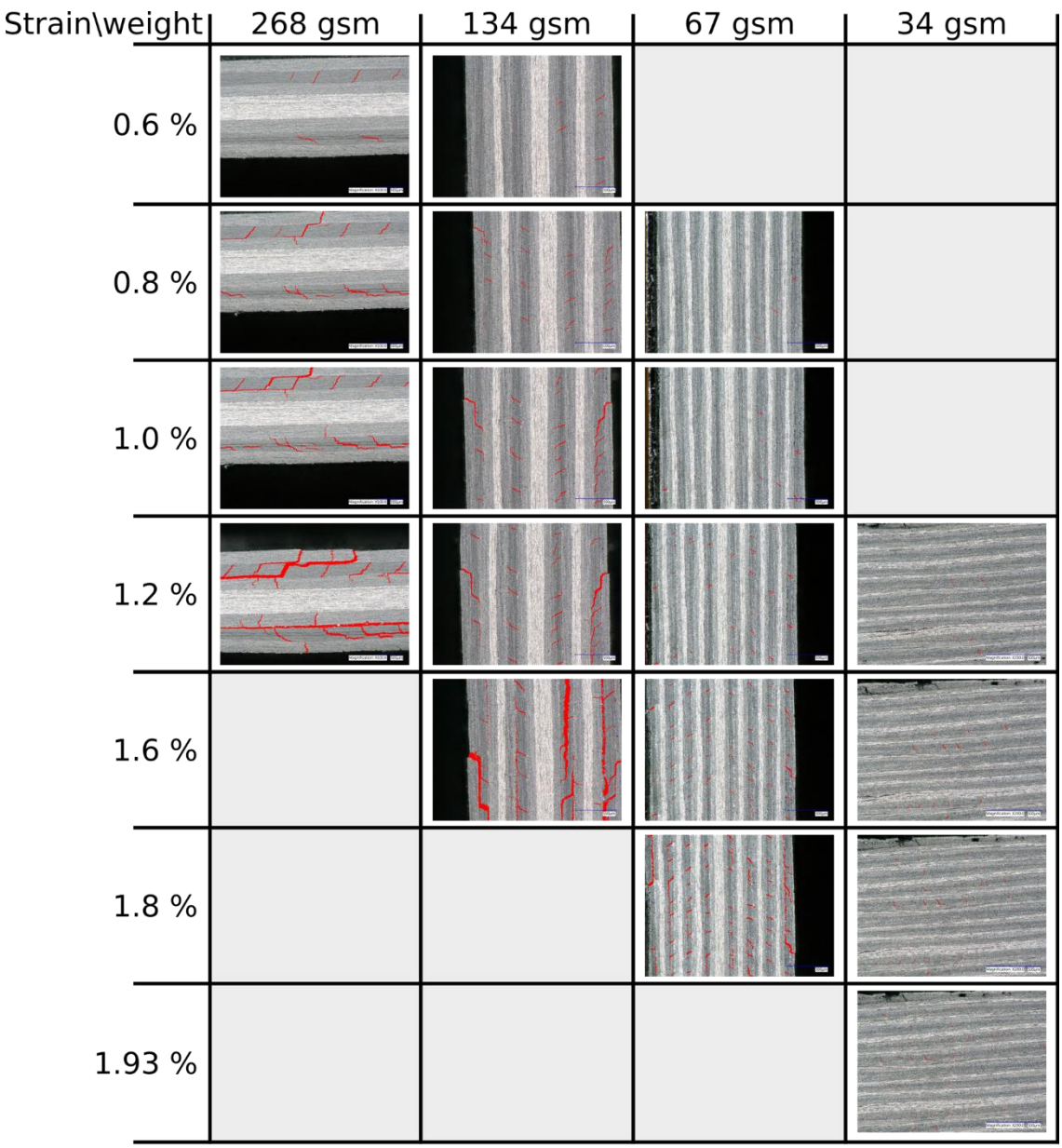

Figure 2: Free edge damage for different ply thicknesses of the T800/TP175 system

In the case of the T800/TP175 system, a similar trend is observed as shown on Fig. 2. Major delamination start growing from 1% strain onwards for the 268gsm samples, eventually leading to the total splitting of the sample prior to failure due to large scale delamination. In the case of the 134gsm samples, the same mechanisms are present, but the delamination is much better contained and no longitudinal splitting of the samples is seen prior to failure. However, the observed final failure mode still exhibits extensive delamination. This large scale delamination is totally absent in the 67gsm samples, where the transverse cracks (the onset of which are delayed) only lead in some instances to limited matrix cracking induced at the tips of the fully developed transverse cracks. The failure mode observed is much more localized. Finally, the 34gsm samples exhibit a much delayed onset of transverse cracking, and no evidence of matrix cracking induced delamination until their failure which happens in a very brittle fashion when the 0° fibre strength is reached.

The evolution of the average transverse crack density observed for each thickness of the T800/TP175 system is shown on Fig. 3. Note here the increased resistance to transverse cracking with decreasing ply thickness which is clearly visible at the start of the curves. The rate of increase of transverse crack density is comparable for all of the three smaller ply thicknesses, where transverse cracking is the dominating damage mode until final failure. In the case of the 268gsm samples, where large scale delamination develops earlier, the growth rate of transverse cracks is naturally decreased. Finally, no saturation of transverse cracks is seen for the 34gsm as the longitudinal fibres fail before this point.

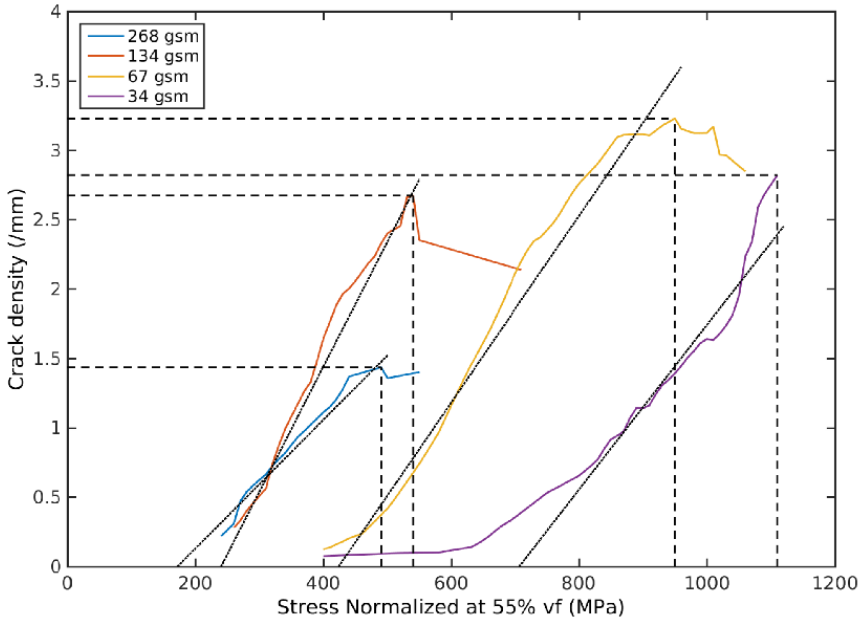

Figure 3: Average crack density for T800/TP175 samples

In order to compare the scaling of the onset of damage with varying ply thickness for both materials, the data are plotted on Fig. 4. The fitted free edge crack scalings follow a typical $1/\sqrt{t}$ relationship, whereas in the case of the M40/TP80 system the acoustic emission is fitted with a linear equation. In both cases, a noticeable difference in both scaling shape and level can be seen between the free edge crack onset and the acoustic emission. For samples made with thicker plies, the free edge damage can be seen to trigger nearly simultaneously the acoustic emission, showing that the free edge damage dominates the samples' global damage behaviour. With decreasing ply thicknesses, the damage propagation into the bulk of the material is delayed, as shown by the growing gap between the acoustic emission onset and the free edge crack onset. Finally, it is observed that the applied stress at which the

free edge crack density saturates for the T800/LME3 system is in very good agreement with the stress at which the acoustic emission threshold is reached.

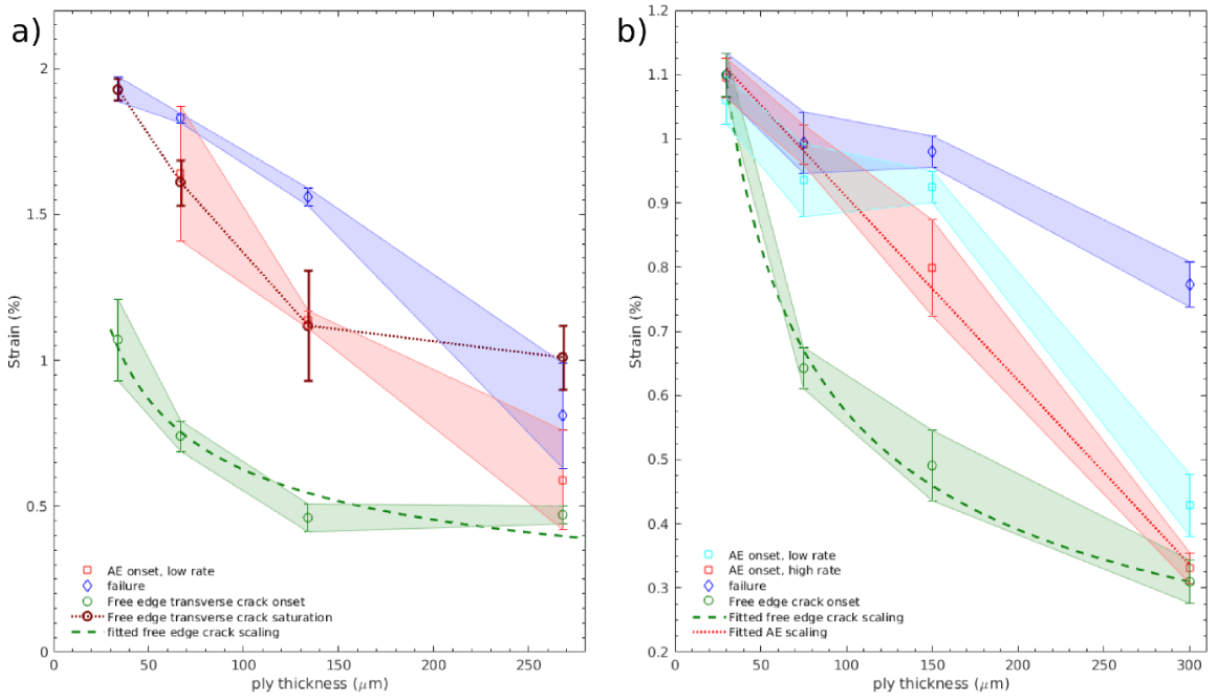

Figure 4: Damage scalings for the T800/TP175 system in a) and the M40/TP80 system in b)

In order to study the propagation of the damage observed at the free edge into the bulk, and thus test the hypothesis that the acoustic emission could be used as a bulk damage predictor, four samples of the M40/TP80 system, two 150gsm and two 100gsm were loaded until 500MPa and 700MPa, respectively 650MPa and 700MPa for tomographic imaging. A typical 90° ply of each specimen is shown on Fig. 5. The loading of the samples pictured on Fig. 5a and 5b was halted before the acoustic emission threshold was reached, whereas the ones pictured on Fig. 5c and 5d have passed it. As highlighted by the difference between both 100gsm specimen which are only separated by 50MPa applied stress, the damage observed at the free edge is constrained there until an applied stress equivalent to the one determined by the acoustic emission threshold is reached, at which point the transverse cracks propagate into the bulk. It can also be noted that the delamination seen at the free edge of the 150gsm sample past acoustic emission (Fig. 5c) is not seen in the sample made of thinner plies at a similar applied stress (Fig. 5d), and that it is constrained to a depth of a few millimetres at most, even when very close to the final failure.

The stress at which the first cracks appear in the numerical model are reported on Fig. 6, and compared to the experimental results. A very good agreement between the experimental and numerical results is found, with similar scalings and a clear difference between a plane-strain situation, akin to what is happening in the bulk of the material, and the plane-stress one which is a good approximation of the free edge.

Considering the experimental results, it is interesting to note that their use to back-calculate an in-situ energy release rate G_{IC}, by using the in-situ strength model [1], yielded values that were both an order of magnitude lower than the experimental values obtained by DCB tests and ply thickness dependent. These values are therefore compared with the ones obtained numerically, with the calculation of the in-situ ERR G_{IC} for the 30gsm and 150gsm cases of the plane-strain model. Values of 35.5 J/ m^2 for

the thickest ply and 18.7 J/ m^2 for the thinnest one are obtained, which are in good agreement with the ones obtained from the in-situ strength model which were 41.7 J/m^2 and 15.4 J/m^2 for the 150gsm, respectively the 30gsm samples.

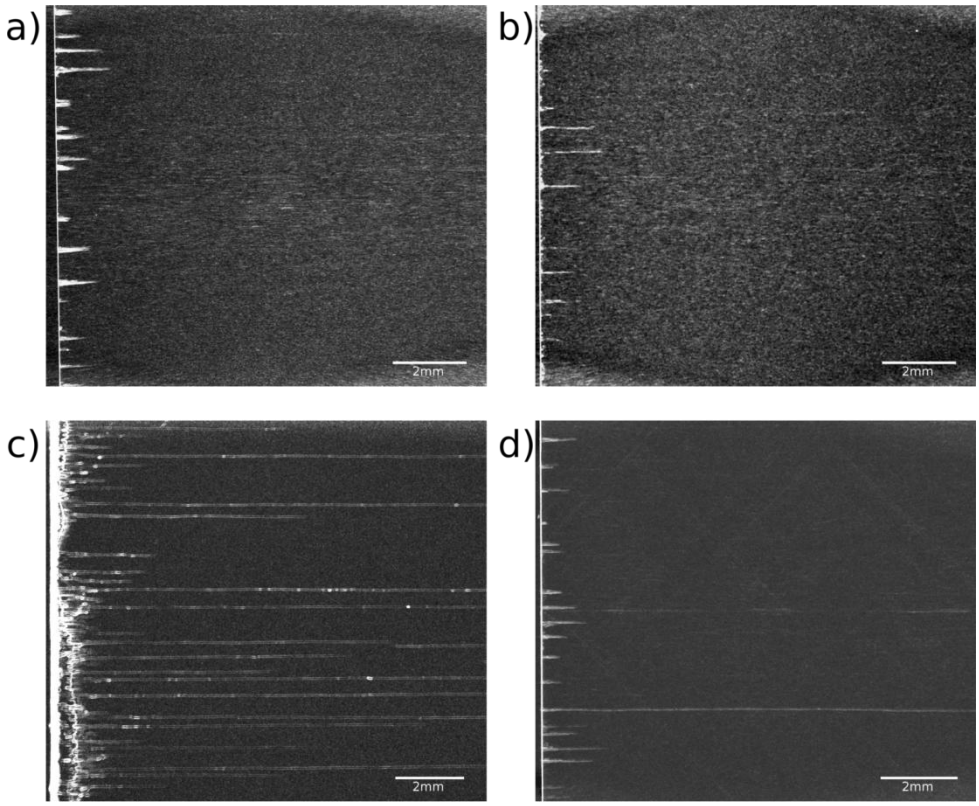

Figure 5: Tomographies of a typical 90° ply in: a) 150gsm at 500MPa; b) 100gsm at 650 MPa; c) 150gsm at 700MPa; d) 100gsm at 700MPa

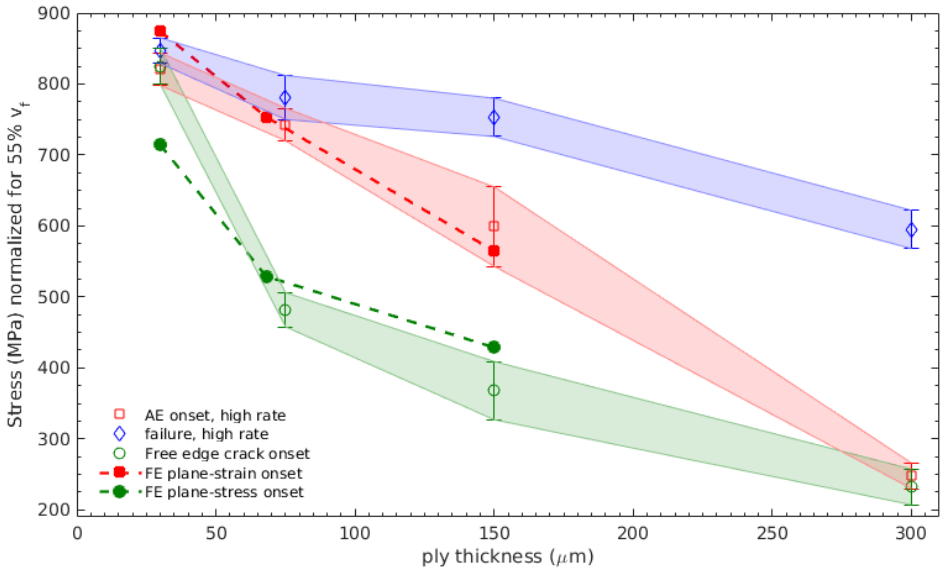

Figure 6: Comparison of the experimental and numerical results for the M40/TP80 system

4. Conclusion

The damage onset and development in quasi-isotropic tensile specimen could be assessed in-situ at the free edge by optical microscopy and in the bulk by acoustic emission. An ex-situ monitoring of the damage growth throughout the width of the sample by x-ray tomography could also be performed. A good agreement was found between the defined acoustic emission cumulative energy threshold, and the propagation of free edge transverse cracks into the bulk of the samples. This also coincided with a saturation of the free edge crack density for samples that were neither dominated by large scale delamination, as are the thickest plies, nor by fibre tensile failure, as is the case for the thinnest ones. Furthermore, it could be shown that the free edge delamination observed in the intermediate ply thicknesses of both materials studied (67, 75, 134 and 150 gsm) remained constrained close to the free edge, at least until the final failure of the samples was triggered.

An apparent in-situ critical energy release rate G_{IC} is estimated from the the acoustic emission onset of damage and the in-situ strength model [1] and it is found to depend on the ply thickness. A similar trend and critical ERR values are found when computing the apparent critical ERR corresponding to first crack growth in the numerical model, which supports the hypothesis of a ply-thickness dependences of the critical ERR associated to transverse cracking. The underlying causes for this dependence as well as the reason for the large difference between these values and the G_{IC} value measured in a DCB test would need further investigation. As such, it explains why the LEFM based analytical model which assumes a constant energy release rate is not able to properly predict the in-situ strength for very thin plies. Finally, at least for quasi-isotropic layups, great care should be exerted when using free edge damage experimental result reports to validate 2D analytical models of the bulk ply failure, as the onset of damage at the free edge was shown to be uncorrelated to the appearance of bulk damage.

Acknowledgements

This research was funded by the Swiss National Science Foundation, project 200021_156207. The authors wish to thank North Thin Ply Technology for the material supply.

References

[1] P.P. Camanho, C.G. Dávila, S.T. Pinho, L. Iannucci, and P. Robinson. Prediction of in situ strengths and matrix cracking in composites under transverse tension and in-plane shear. *Composites Part A : Applied Science and Manufacturing*, 37(2) : 165–176, 2006

[2] R. Amacher, J. Cugnoni, J. Botsis, L. Sorensen, W. Smith, and C. Dransfeld. Thin ply composites : Experimental characterization and modeling of size-effects. *Composites Science and Technology*, 101 : 121– 132, 2014.

[3] S. Kohler, R. Amacher, J. Cugnoni and J. Botsis. Damage mechanisms in thin-ply composites: Free edge and bulk measurements compared to multiscale modelling. *Proceedings ECCM17*, 2016.

[4] F. Sket, A. Enfedaque, C. Alton, C. González, J.M. Molina-Aldareguia and J. Llorca. Automatic quantification of matrix cracking and fiber rotation by X-ray computed tomography in shear-deformed carbon fiber-reinforced laminates. *Composites Science and Technology*, 90 : 129-138, 2014

[5] A.R. Melro, P.P. Camanho, F.M. Andrade Pires, and S.T. Pinho. Micromechanical analysis of polymer composites reinforced by unidirectional fibres : Part I - constitutive modelling. *International Journal of Solids and Structures*, 50(11-12) : 1897–1905, 2013.